



www.asianpubs.org

ARTICLE

Effect of Copper Oxide on Structural, Optical and Photocatalytic Activity of Reduced Graphene Oxide for Eosin B

C.C. Vidyasagar¹, Prakash Kariyajjanavar²,
Gururaj Hosamani³, Priya Nikkam¹, Keerti M. Khilari¹,
Veena Mathapati³ and Megha Madiwalar¹

ABSTRACT

Nowadays incorporation of few oxygen groups between the layers of graphite have shown potential approach for industrialization of graphene oxide for different potential applications. During the strong oxidation process in modified Hummers method, these oxygen based functional groups may increase the distance, weakening the van der Waals forces and facilitation the exfoliation of graphite layers from. The reduced graphene oxide/copper oxide (rGO-CuO) is highly potentially active and selective catalyst for many environmental applications. Different wt. % of Cu(II) and loaded on rGO surface to form a nanocomposite, which were prepared by hydrothermal method. The influence of hydrothermal temperature, rGO sheet and loaded CuO on structure of graphene was systematically investigated. The structure and optical properties of the obtained hybrid composite was evaluated employing scanning electron microscope, X-ray diffraction, UV-visible and infrared spectroscopies. The photocatalytic activities of rGO-CuO nanocomposites for the degradation of Eosin B acid red under sunlight were investigated. The results revealed the decrease in percentage photocatalytic degradation rate occurred on rGO-CuO, because a single sheet of rGO can shield the light from reaching the surface of CuO photocatalyst. It is possible to provide a new way to use the host rGO as prepared by hydrothermal method for water remediation applications.

KEYWORDS

Degradation, Eosin Blue, Hummer's method, Photocatalyst, Reduced graphene oxide/copper oxide.

INTRODUCTION

In recent years, increasing attention has been paid to the development of advanced materials due to environmental concerns. Recent textile industries have become a source of pollutants extracted from the cotton fibre during the process of chemicals and the dyes, which discharges to the environment. This may cause aesthetic problems due to the unprocessed industrial effluents. The treatment of industrial effluents are difficult with present conventional biological and chemical process, because of non-degradable nature of most dyes in environmental conditions, due to highly structured polymers with low biodegradability [1,2]. However, various physico-chemical techniques, such as adsorption on activated carbon and ultra filtration are limited to low concentration ranges [3,4].

Asian Journal of Materials Chemistry

Volume: 4 Year: 2019
Issue: 3-4 Month: July-December
pp: 34-42
DOI: <https://doi.org/10.14233/ajmc.2019.AJMC-P77>

Received: 4 August 2019
Accepted: 15 October 2019
Published: 26 December 2019

Author affiliations:

¹Department of Chemistry, Rani Channamma University, Belgaum-591156, India

²Department of Environmental Science, Gulbarga University, Kalaburagi-585106, India

³Department of Electronics, Government First Grade College, Channaraypatna-573116, India

[✉]To whom correspondence to be addressed:

E-mail: vidya.891@gmail.com

Available online at: <http://ajmc.asianpubs.org>

Recently, the photocatalytic degradation of industrial effluents has become a progressively significant process for water treatment and air purification. This process has a potential to decompose dyes into non-toxic substances under visible light irradiation. It is essential to develop an efficient photocatalyst for industrial effluents under visible light irradiation [5-7]. Graphene has strong absorption over the solar spectrum, especially in the near IR region, and it is the most thermally conductive material known so far [8]. Graphene has attracted considerable interest in the recent years because of its strong absorption over solar spectrum near IR region and photocatalytic properties [9-11]. Due to its unique physico-chemical and intriguing properties such as high mobility of charge carriers, unique transport performance [12-14], high mechanical strength [15], extreme high thermal conductivity and theoretically more surface area of 2600 m²/g [16]. The toxicity of different forms and hybrids of graphene is suitable for many potential applications such as sensors [17-20], energy conversion devices [21,22], catalysts [23] and degradation of dyes [24]. Till date, the most efficient synthetic method have been based on exfoliation of graphite [25,26]. The major difference between them is the yield and the defect content of their products [27]. Hence, a material chemist need to trial and error the synthetic techniques to control size, shape and morphology of a graphene based hybrid material. Soon after Hummer's report, several chemists modified the synthesis of graphene from graphite under strong oxidants with certain reaction conditions [13,28]. In literature, there are various methods reported on synthesis of graphene oxide based hybrid materials and their derivatives, which include mechanical cleavage of graphite [29], chemical exfoliation of graphite [25], solvothermal synthesis [18], epitaxial growth on substrates [20], sonochemical approach [30], environment-friendly greener reduction method [31] and hydrothermal methods [29]. Among these different approaches, direct Hummer's modified hydrothermal treatment is an effective approach to synthesize graphene based hybrid materials in order to tailoring the required properties [18,32]. More importantly, exfoliated GO sheets frequently possess a wealthy assortment of oxygen-containing groups in GO allows interactions with cations and provide reactive sites for the nucleation and growth of metal oxides, which results in crystal growth of various graphene-based composites [32]. Up to now, several excellent graphene based metal oxides have been synthesized and supported on graphene, which include CuO [33,34], NiO [32], TiO₂ [35], SnO₂ [36], MnO₂ [37], Fe₃O₄ [38], ZrO₂ [39] and Cu₂O [18], *etc.* Recently, GO was modified with metal oxides using numerous methods. The graphene oxide nanocomposites and functional nanomaterials are expected to produce a material with improved performance *via* possible synergetic interaction. Recent reports attracted increasing number of researchers in the field have been committed in to the incorporation of graphene into composite materials, including metal nanoparticles [40], metal oxides [25] quantum dots [41], polymers [42]. Among that material, copper oxides has received a great deal of consideration because of its superior electrochemical stability and electrocatalytic activity as well as low cost for extensive applications [43]. Therefore, anchoring metal oxides in graphene oxide will boost the efficiency in various dyes degradation applications. Many scientists have

studied the preparation of graphene oxide-metal oxide nanocomposite for the degradation of dyes, adsorption and other contamination removal from water. Till date numerous rGO-MO nanocomposites were effectively studied for degradation of methylene blue [44], rhodamine B [45], methyl orange [10]. In this article, we discussed preparation of reduced graphene oxide and its hybrid materials for their potential application of industrial textile dye (Eosin B) degradation. We focussed on the design of graphene oxide/CuO hybrid materials, which is an important application for environmental remediation. Herein, we emphasize the hydrothermal preparation of reduced graphene oxide hybrid material and characterization of rGO-CuO composites.

EXPERIMENTAL

Eosin Blue (acid red) dye was procured from Dye star company, Mumbai, India and the natural graphite powder was procured from Merck, Mumbai, India. The chemicals *viz.* sodium nitrate (97 %), hydrogen peroxide (30 wt. %), sulphuric acid (98 %), potassium permanganate, copper(II) nitrate and sodium hydroxide were used for the preparation of composites. Double distilled water was used for the preparation of stock solutions. All the chemicals were of analytical grade and used as received without further purification.

Preparation of reduced graphene oxide (rGO): The reduced graphene oxide (rGO) is prepared by modified Hummer's method. To exfoliate the preoxidized graphite powders into few layer GO sheets, the expanded graphite powder (2 g) and 15 g KMnO₄ was added into cold H₂SO₄ (120 mL) under stirred for 2 h. The solution was diluted by water (250 mL), then 20 mL H₂O₂ (30 %) added to reaction mixture at room temperature. The reaction mixture kept for stirring for 12 h, the upper supernatant was collected and centrifuged, where the rGO powders were obtained as precipitates. HCl solution was added to remove the metal (Mn²⁺) ions existing in the GO powders. Finally, rGO was washed many times with deionized water till it reaches pH 7.

Preparation of rGO-CuO composites: Hydrothermal is a powerful tool for the synthetic inorganic materials, which operates at an elevated temperature in a confined volume to generate high pressure. An rGO-CuO composite with controlled crystal facets can be easily obtained by controlling the experimental parameters such as concentration of precursor solution and the reaction time using the hydrothermal method. A mixture of 5 mL of Cu(NO₃)₂·3H₂O and 50 mL of graphene oxide (dispersed in water) was taken in 250 mL beaker and it was stirred about 1 h. Then the composite was annealed at 200 °C in autoclave for 2 h. The resultant colloidal solution was filtered several times by double distilled water.

Characterizations: The XRD patterns were recorded on a Philips X'Pert X-ray diffractometer using Cu-K α radiation. High resolution transmission electron microscopic (HRTEM) analysis of the samples have been carried out to investigate the morphology of synthesized materials using JEOL microscope [Model JEM 3010] operated at 300 kV. Elemental analysis was done on an energy dispersive X-ray spectroscopy (EDAX) [model: Nova Nano SEM600-FEI]. The optical properties and photo response of composites were measured on a UV-Vis spectrophotometer [model: USB 4000, Ocean Optics, USA].

RESULTS AND DISCUSSION

Structural analysis: The structure of GO, CuO, rGO and rGO/CuO composites were characterized by powder X-ray diffraction. The X-ray diffraction patterns of the as-synthesized GO and rGO peaks were observed at $2\theta = 11.8^\circ$ and 24.5° corresponding to the (0 0 1) plane, respectively. The larger interplanar spacing of GO (Fig. 1a) was found to be 0.75 nm compare to rGO ($d = 0.36$ nm), this might be due to the introduction of oxygen-containing functional groups such as hydroxyl, carboxyl on the GO sheets. After chemical reduction of GO, the FWHM for rGO was found to be broader with a large shift towards higher 2θ angle (24.5°) with interplanar spacing of about 0.36 nm, signifying the occurrence of residual oxygen containing groups on rGO sheets (Fig. 1c). The FWHM of the diffraction peaks give information about the crystallinity of the stacking regularity of the layers. It has been observed that in the presence of residual oxygen containing functional groups, it will lead to the formation of shorter interplanar spacing ($d = 0.36$ nm) between the layers compare to GO ($d = 0.75$ nm), which could be reason for increase in the FWHM of diffraction peaks for rGO. This suggests that the oxygen containing functional groups of GO could be significantly converted into rGO at 200°C by hydrothermal method. Copper is an important material because of their catalytic and electrical conducting properties, which is known as p-type semiconductor exhibiting narrow band gap ($E_g = 1.2$ eV). The major peaks of CuO located at 2θ values correspond to monoclinic phase and all the peaks are well assigned to JCPDS card No. 80-1268. No other peaks were observed belonging to any impurity such as $\text{Cu}(\text{OH})_2$ and Cu_2O particles. For samples of rGO-CuO, no diffraction peaks of layered GO can be seen, signifying the deficiency of layer-stacking regularity after chemical reduction by the cations. On the other hand, in rGO-CuO exhibit high intensity by slightly shifting peaks towards lower 2θ angle from 24.5 to 18.8° with increasing interplanar spacing (0.47 nm) (Fig. 1d)

compare to rGO (0.36 nm) (Fig. 1c), due to the interaction of crystalline CuO between the rGO layers. Sometimes traces of residual oxyginate groups on rGO-CuO is believed to be favourable for maintaining a good dispersion of the composite nano sheets. Graphene oxide is in the form of a composite and the CuO phase dominates the GO layers. This conclusion is supported by TEM studies of rGO-CuO. Fig. 2(a-b) show the surface morphology of rGO (looks like folded graphene sheet) and rGO-CuO (looks like CuO particles on folded graphene sheet), respectively. After combination with GO to form a rGO-CuO composite, the CuO nanoparticles are firmly anchored on the rGO layers with a high density with sizes ranging from below 100-200 nm. The rGO may favour the hindrance of CuO from agglomeration and enable their good distribution, whereas CuO serves as a stabilizer to separate GO sheets against aggregation. The TEM images of rGO-CuO as shown in Fig. 2b revealed that the composite consists of a large amount of CuO nanoparticles with sizes

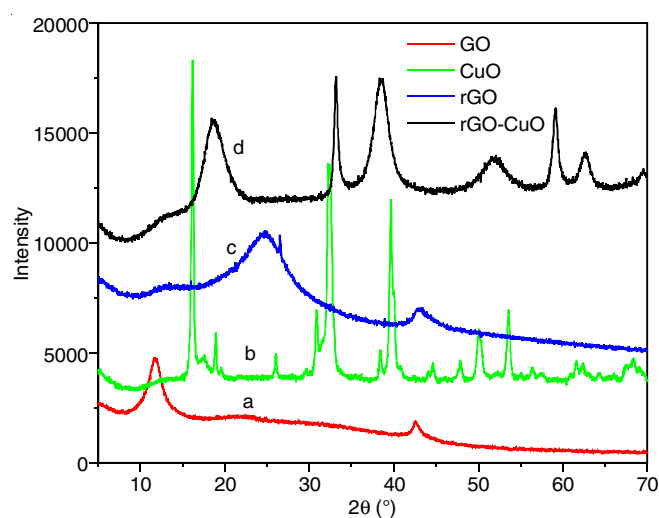


Fig. 1. XRD patterns of samples GO, CuO, rGO and rGO-CuO

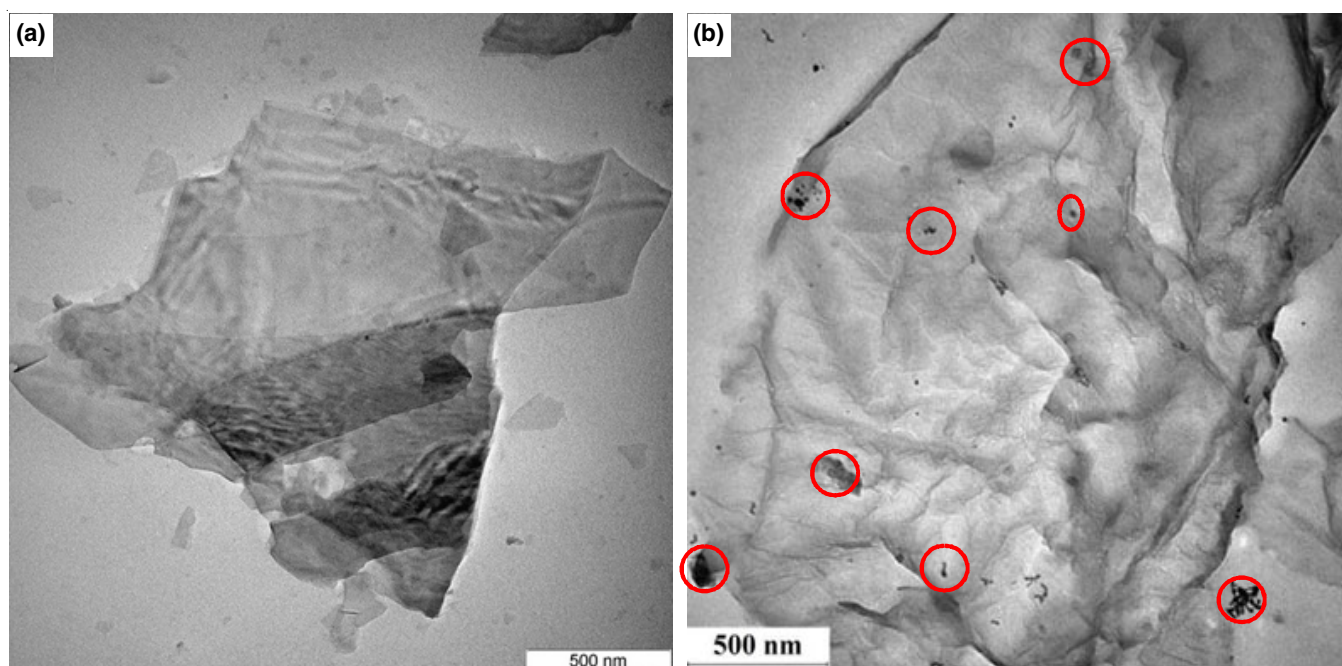


Fig. 2. TEM images of as-synthesized (a) rGO and (b) rGO-CuO composites

ranging from 100 to 200 nm. The GO shows an ultra-thin wrinkled paper-like structure and the CuO nanoparticles tend to aggregate on rGO sheets with size of 100-200 nm. As observed, CuO nanoparticles are spread across the sheet with intimate contact. Table-1 shows the XRD data of as-prepared samples GO and rGO-CuO.

Optical properties: The effect of graphene oxide/metal oxide composite was studied using UV-visible spectra, to study the effect of metal oxide on graphene oxide, GO/MO powder was grounded with a mortar and pestle and dispersed in 50 mL of double distilled water. Fig. 3 shows the ultraviolet-visible spectra of graphite and graphene oxide. The spectrum of graphene oxide has a characteristic absorption shoulder peak at 235 nm, this blue shift is due to splitting of graphene layers from graphite and corresponds to a $\pi-\pi^*$ of aromatic C=C ring. Formation and stability of graphene oxide nanoparticles in sterile distilled water is confirmed using UV-visible spectroscopy in a range of wavelength from 250 nm to 300 nm (Fig. 4). However, the unique highly electronic properties of graphene are due to its π -electron cloud (puddle) formation, which has 97.4 % optical transmittance.

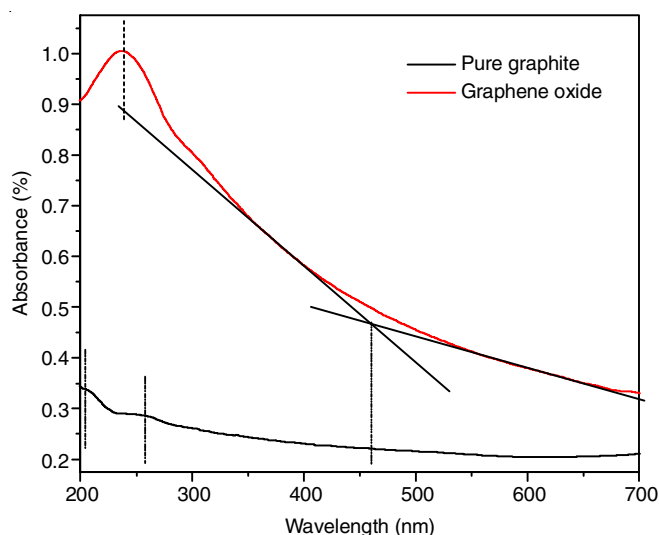


Fig. 3. UV-visible absorption spectra of pure graphite and graphene oxide nanoparticles were synthesized by Hummer's method

Infrared analysis: Fig. 5 shows the IR spectra GO, CuO, rGO and rGO-CuO nanocomposites. For GO, the peak at 3418 cm^{-1} corresponds to O-H stretching vibration. The peak at 1633 cm^{-1} is attributed to C=C stretching vibration. The absorption

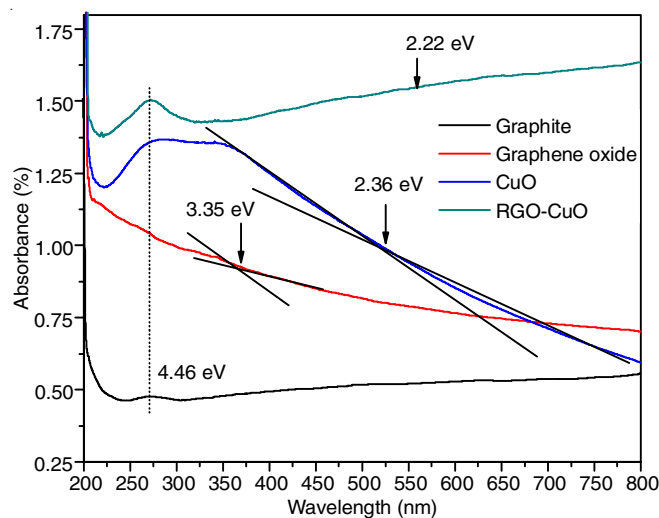


Fig. 4. UV-visible absorption spectra of pure graphite, graphene oxide, copper oxide and reduced graphene oxide/CuO composite were synthesized by Hummer's method

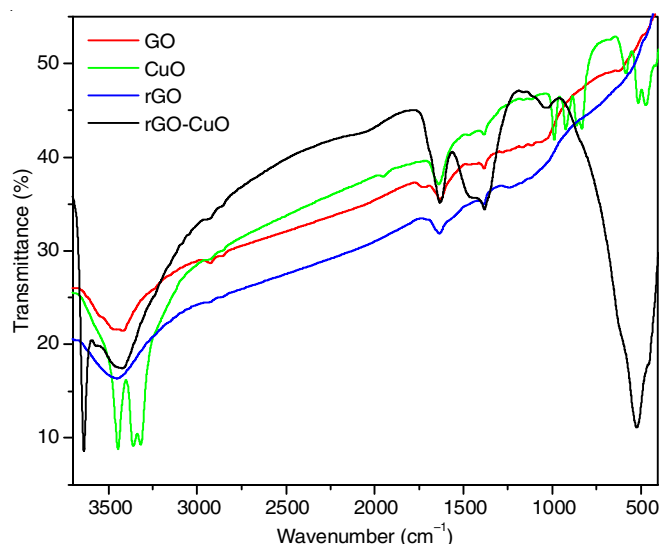


Fig. 5. IR spectra of GO, CuO, rGO and rGO-CuO nanocomposites

peak at 1720 cm^{-1} is attributed to C=O group. The absorptions peaks at 2934 cm^{-1} represent the symmetric stretching vibrations of C-H. The absorption peaks at 1384 cm^{-1} and 1166 cm^{-1} are ascribed to the stretching vibration of CH_3 and C-OH of alcohol, respectively, which was used for washing purposes.

TABLE-1
XRD DATA OF AS-PREPARED SAMPLES GO AND rGO-CuO

Samples	2 θ	Intensity	FWHM	d-Spacing (\AA)	Rel. Int. (%)
Graphene oxide	11.6401	1878.73	0.3306	7.60260	100
	42.5497	569.19	0.4032	2.12296	30.3
rGO	43.2646	258.92	0.84	2.08952	100
CuO	16.2563	13482.5	0.2214	5.45263	100
	32.4194	9421.11	0.15	2.75941	69.88
	39.6678	8046.65	0.1968	2.27218	59.68
	53.6189	2914.58	0.1968	1.70930	21.62
rGO-CuO	33.1241	5130.73	0.246	2.70453	100
	59.1706	3397.43	0.1722	1.56149	66.22
	62.6087	1237.00	0.7872	1.48376	24.11
	69.4811	416.52	0.492	1.35285	8.12
	72.7568	591.95	0.96	1.29873	11.54

For rGO-CuO, the peak at 3454 cm^{-1} corresponds to O-H stretching vibration. The absorptions peaks at 2924 , 2824 and 2360 cm^{-1} represent the symmetric stretching vibrations of C-H. The peak at 1744 cm^{-1} is attributed to C=O stretching vibration. The absorption peak at 1634 cm^{-1} is attributed to C=C group. The absorption peaks at 1464 and 1166 cm^{-1} are ascribed to the stretching vibration of CH_2 and C-OH of alcohol, respectively. The absorption peaks 495 cm^{-1} is ascribed to CuO. All the frequencies of IR groups are shown in Table-2. The characteristic peaks of both components can be seen in the spectra of composite material. Hence, the FTIR results revealed the anchoring of CuO nanoparticles on the surface of rGO sheets.

Photocatalytic studies of eosin B (acid dye): The degradation of solar light active rGO-CuO nanocomposite towards eosin B dye as model organic pollutant was evaluated. The aqueous solution of eosin B (Aldrich) with a concentration of 5 ppm was prepared. In each experiment 5 ppm (20 mL) eosin B solution and 10 mg of rGO were added into a test tube (10 mL) and sonicated for 10 min. The photocatalysis experiment was carried out under sun light from 11 am to 2 pm. After keeping a steady state in dark by wrapping aluminium foil for 15 min and each irradiating for 0, 10, 20, 30 and 40 min. A solution

(2 mL) were taken out and subsequently measured their absorbance on UV-visible spectrophotometer. Fig. 6 shows the degradation spectra of eosin B dye by bare rGO and rGO-CuO nanocomposites within 40 min. The maximum absorption peak of eosin B dye occurring at 518.9 nm is decreased continuously during the exposure time, suggesting that eosin B dye was gradually photodegraded by rGO (Fig. 6a) and rGO-CuO (Fig. 6b), respectively. As CuO nanoparticles are uniformly dispersed on the surface of rGO sheet (Fig. 2b), primarily the adsorption of eosin B would form on the surface of folded rGO as well as CuO nanoparticles. The charge separation occurs following the exposure of the surface of catalyst (rGO-CuO) by solar light, the electrons and holes could migrate to the catalyst surface where they participate in redox reaction with dye species. As rGO-CuO is a p-type semiconductor, there is a majority of holes (h^+) in valence band and less number of electrons (e^-) in conduction band. Holes could react with H_2O or OH^- to produce the hydroxyl radicals and electrons will be picked up by oxygen to generate superoxide radicals (O_2^-) as described in the following equations:

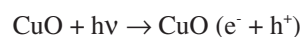


TABLE-2
KEY INFRARED FREQUENCIES OF AS-PREPARED SAMPLES GO AND rGO-CuO

S. No	GO			rGO-CuO		
	Groups	Frequency (cm^{-1})	Intensity	Groups	Frequency (cm^{-1})	Intensity
1	O-H	3418.58	Strong	O-H	3454.44	Strong
2	C-H stretch	2925.33	Weak	C-H stretch	2924.57	Weak
3					2839.9	Weak
4	C=C	—	—	—	2360.53	Strong
5	C=O	1720.11	Weak	C=O	1744.84	Weak
6	C=C arom.	1633.49	Strong	C=C arom.	1634.95	Strong
7	C-H bend	1384.04	Weak	C-H bend	1464.19	Weak
8	C-O-C stretch	1166.72	Weak	C-O-O stretch	1165.36	Weak
9				Cu-O	605.04	Weak
10				Cu-O	495.99	Strong

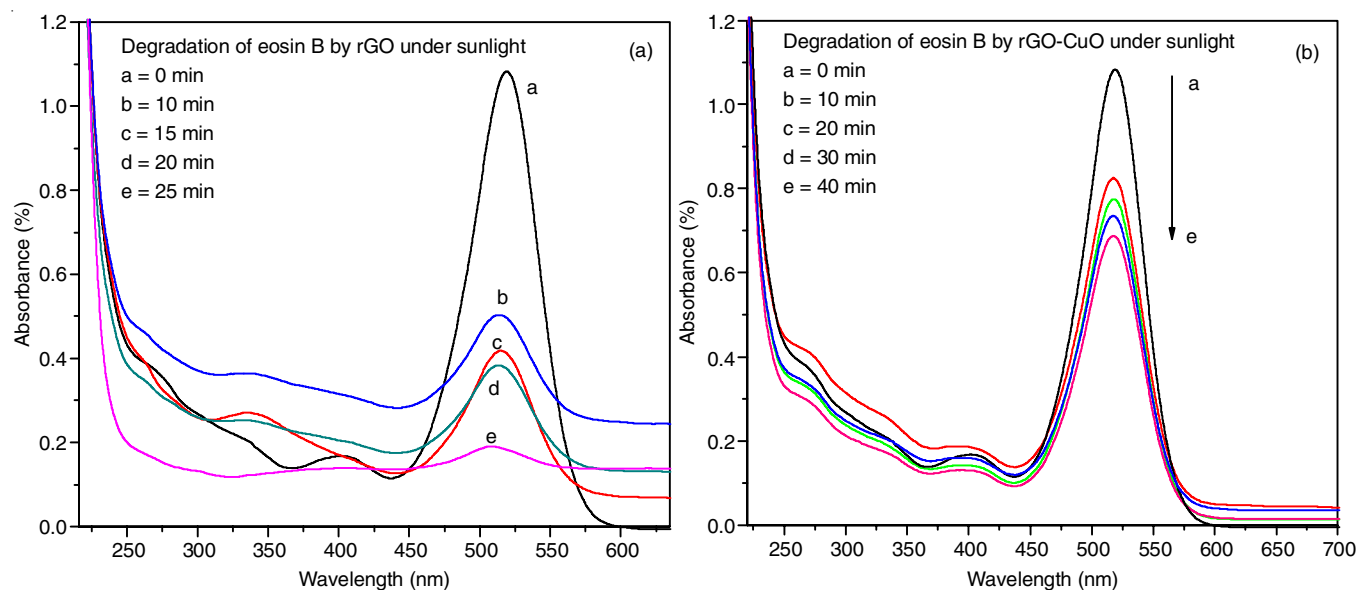


Fig. 6. UV-visible absorption spectra for photocatalysis reaction of eosin blue (a) rGO with eosin blue and (b) rGO-CuO composite with eosin blue for different time of solar light illumination

recombination rate is more due to smaller band gap of CuO



electron hole pairs are less on the surface of folded rGO catalyst

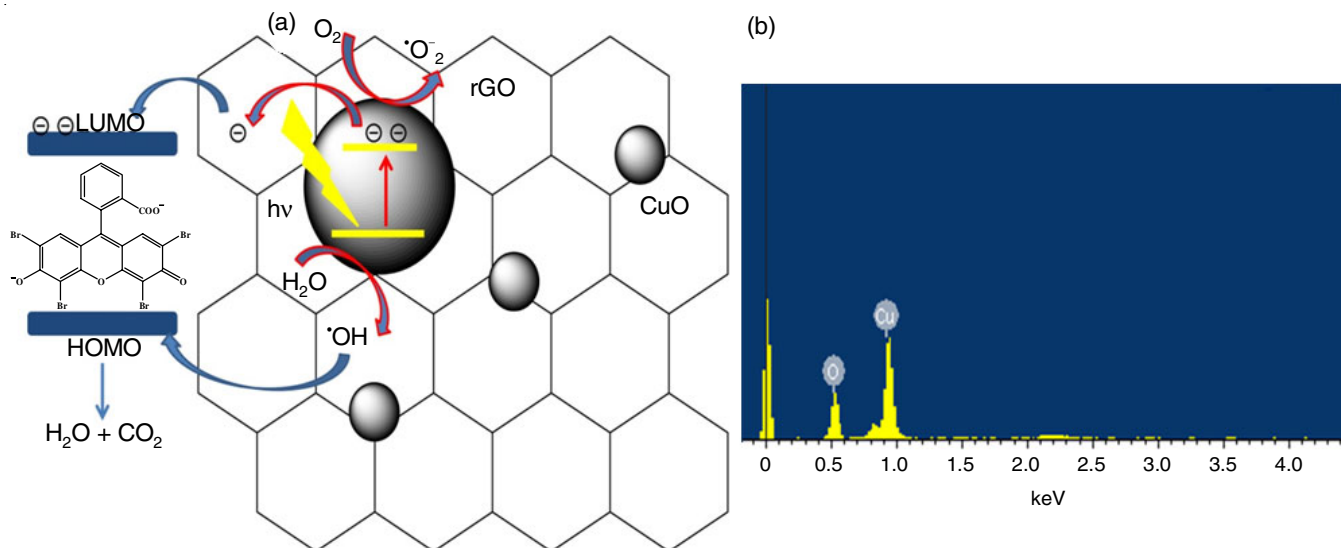
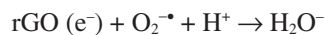


Fig. 7. Proposed mechanism of photocatalytic degradation of eosin blue using rGO-CuO composite (a) and EDAX pattern of as prepared rGO-CuO

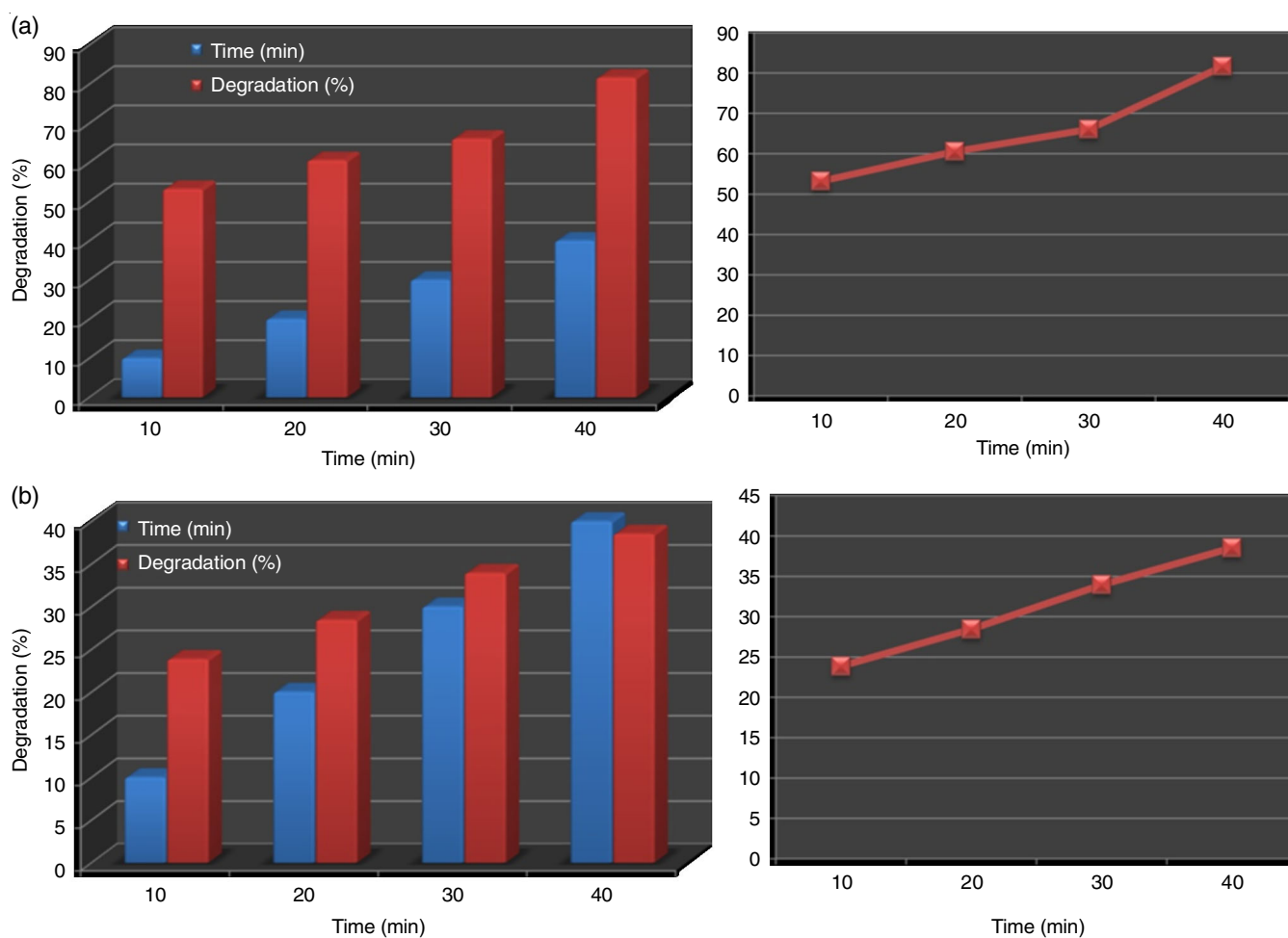


Fig. 8. Comparison of the photodegradation efficiency (a) rGO with eosin blue and (b) rGO-CuO composite with eosin blue at 10, 20, 30 and 40 min of solar light illumination in between 12.30 to 13.10 pm

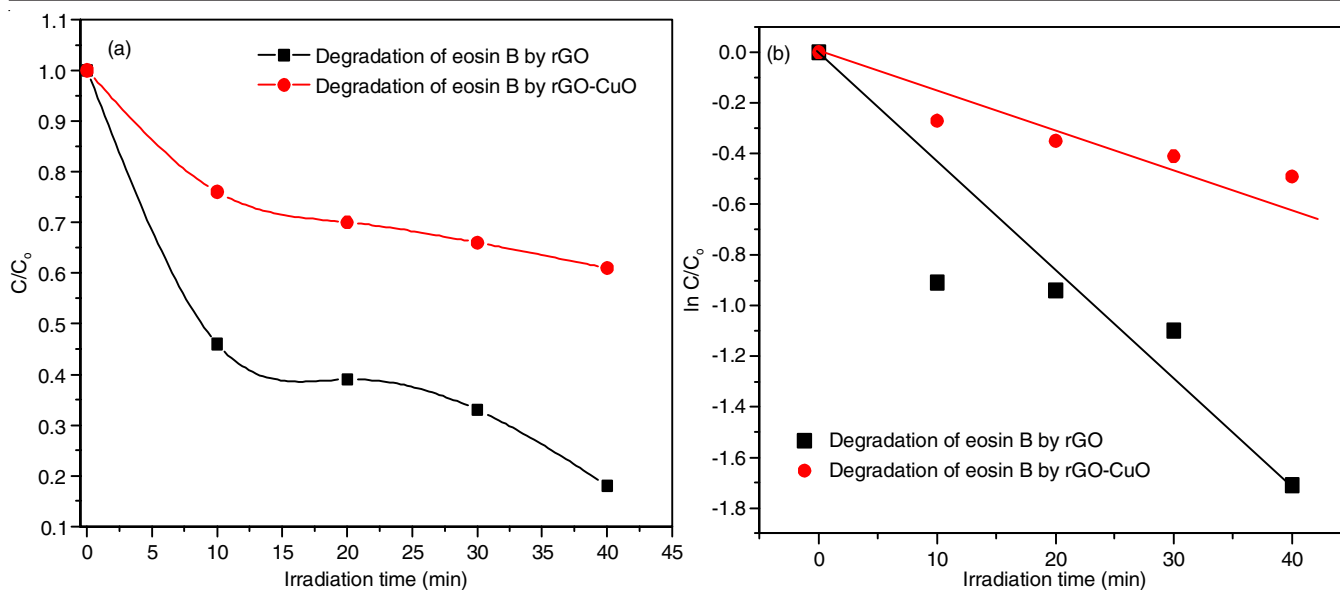


Fig. 9. Photocatalytic kinetic degradation of profiles of eosin blue using rGO and rGO-CuO under solar light illumination in between 12.30 to 13.10 pm

Since rGO interacts strongly with eosin B due to its π -conjugated planar surface. A enhanced surface area of rGO has been found as compared to that of rGO-CuO nanoparticles, which improves the uptake of eosin B from water and a degradation mechanism can be predicted (Fig. 7a). The EDAX analysis was employed to evaluate the CuO nanoparticles on the surface of rGO nanosheets (Fig. 7b). No other peaks were observed for impurities, which is the evidence for the presence of carbon, oxygen and copper in rGO-CuO catalyst. It is quite evident from Fig. 8a-b that the rGO has the highest photocatalytic efficiency and it is decomposed 80 % in just 40 min under solar light illumination, whereas photocatalytic degradation for rGO-CuO composite was found to be 37 % in 40 min. The enhancement in photodegradation of eosin B dye by rGO has shown higher photocatalytic property than that of rGO-CuO composites, because of unfolded large surface area and 2D structure of rGO as indicated by TEM images (Fig. 2a). From Fig. 8, it is obvious that the maximum photocatalytic activity was achieved with the rGO loading against eosin B, indicating that rGO can effectively promote the charge separation on interface and improve the photocatalytic performance significantly. The decrease in percentage photocatalytic degradation rate occurred on rGO-CuO, because a single sheet of rGO can shield the light from reaching the surface of CuO photocatalyst. The most of the photocatalytic degradation fits in pseudo-order kinetics model. The kinetic $\ln C/C_0$ linear curve for the degradation of eosin B under solar light illumination follows the pseudo first-order kinetics as per Langmuir-Hinshelwood model. The plot C/C_0 as a function of irradiation time for all the samples is shown in Fig. 9.

Conclusion

As concluded in this work, the rGO-CuO composite was successfully synthesized by modified Hummer's method followed by hydrothermal method. As synthesized nanocomposite was confirmed by XRD, TEM, UV-vis and IR spectroscopic

studies. The rGO was found to have high and extended light absorption range, enhanced charge separation and transportation properties than rGO-CuO, because of less band gap and high recombination rate in CuO. From the TEM images, it is understandable that CuO is topping on the basal plane of the folded rGO and hence agglomerations were found in rGO-CuO. The decrease in percentage photocatalytic degradation rate occurred on rGO-CuO, because a single folded sheet of rGO can shield the light from reaching the surface of CuO photocatalyst. It would be better to use metal oxides having higher band gaps with rGO for the degradation of dyes.

ACKNOWLEDGEMENTS

The authors are grateful to Rani Channamma University, Belagavi, India and The VGST (Vision Group on Science and Technology, Government of Karnataka, Bangalore, India) (VGST-SMYSR/GRD-429) for the financial support. The authors are also thankful to Indian Institute of Science, Bangalore, India for providing XRD, TEM and EDAX analyses.

REFERENCES

1. J.D. Bracken, The History and Use of Our Earth's Chemical Elements: A Reference Guide (Krebs, Robert E.), *J. Chem. Educ.*, **76**, 475 (1999); <https://doi.org/10.1021/ed076p475>.
2. A. Anouzla, Y. Abrouki, S. Souabi, M. Safi and H. Rhabal, Colour and Cod Removal of Disperse Dye Solution by a Novel Coagulant: Application of Statistical Design for the Optimization and Regression Analysis, *J. Hazard. Mater.*, **166**, 1302 (2009); <https://doi.org/10.1016/j.jhazmat.2008.12.039>.
3. D. Cailan, C. Teodosiu and F. Brinza, Studies Regarding Advanced Processes Used for Reactive Dyes Removal From Textile Effluents, *Environ. Eng. Manag. J.*, **8**, 1045 (2009); <https://doi.org/10.30638/eemj.2009.154>.
4. C. Thamaraiselvan, M. Noel, Membrane Processes for Dye Wastewater Treatment: Recent Progress in Fouling Control, *Crit. Rev. Environ. Sci. Technol.*, **45**, 1007 (2015); <https://doi.org/10.1080/10643389.2014.900242>.

5. K. Rajeshwar, M.E. Osugi, W. Chanmanee, C.R. Chenthamarakshan, M.V.B. Zanoni, P. Kajitvichyanukul, R. Krishnan-Ayer, Heterogeneous Photocatalytic Treatment of Organic Dyes in Air and Aqueous Media, *J. Photochem. Photobiol. C Photochem. Rev.*, **9**, 171 (2008); <https://doi.org/10.1016/j.jphotochemrev.2008.09.001>.
6. H.Y. Shu, C.R. Huang, Degradation of Commercial Azo Dyes in Water using Ozonation and UV Enhanced Ozonation Process, *Chemosphere*, **31**, 3813 (1995); [https://doi.org/10.1016/0045-6535\(95\)00255-7](https://doi.org/10.1016/0045-6535(95)00255-7).
7. R. Li, F. Zhang, D. Wang, J. Yang, M. Li, J. Zhu, X. Zhou, H. Han and C. Li, Spatial Separation of Photogenerated Electrons and Holes Among {010} and {110} Crystal Facets of BiVO₄, *Nat. Commun.*, **4**, 1432 (2013); <https://doi.org/10.1038/ncomms2401>.
8. A.C. Neto, F. Guinea and N.M. Peres, Drawing Conclusions from Graphene, *Phys. World*, **19**, 33 (2006); <https://doi.org/10.1088/2058-7058/19/11/34>.
9. S. Stankovich, D.A. Dikin, G.H.B. Dommett, K.M. Kohlhaas, E.J. Zimney, E.A. Stach, R.D. Piner, S.B.T. Nguyen and R.S. Ruoff, Graphene-Based Composite Materials, *Nature*, **442**, 282 (2006) <https://doi.org/10.1038/nature04969>.
10. Q. Xiang, J. Yu and M. Jaroniec, Graphene-Based Semiconductor Photocatalysts, *Chem. Soc. Rev.*, **41**, 782 (2012) <https://doi.org/10.1039/C1CS15172J>.
11. A.H. Castro Neto, F. Guinea, N.M.R. Peres, K.S. Novoselov and A.K. Geim, The Electronic Properties of Graphene, *Rev. Mod. Phys.*, **81**, 109 (2009); <https://doi.org/10.1103/RevModPhys.81.109>.
12. N. Salam, A. Sinha, A.S. Roy, P. Mondal, N.R. Jana and S.M. Islam, Synthesis of Silver-graphene Nanocomposite and Its Catalytic Application for the One-pot Three-component Coupling Reaction and One-Pot Synthesis of 1,4-Disubstituted 1,2,3-triazoles in Water, *RSC Adv.*, **4**, 10001 (2014); <https://doi.org/10.1039/c3ra47466f>.
13. K.S. Novoselov, A.K. Geim, S. V. Morozov, D. Jiang, Y. Zhang, S. V Dubonos, I. V Grigorieva and A.A. Firsov, Electric Field Effect in Atomically Thin Carbon Films, *Science*, **306**, 666 (2004); <https://doi.org/10.1126/science.1102896>.
14. X. Du, I. Skachko, A. Barker, E.Y. Andrei, Approaching Ballistic Transport in Suspended Graphene, *Nat. Nanotechnol.*, **3**, 491 (2008); <https://doi.org/10.1038/nnano.2008.199>.
15. C. Lee, X. Wei, J.W. Kysar and J. Hone, Measurement of the Elastic Properties and Intrinsic Strength of Monolayer Graphene, *Science*, **321**, 385 (2008); <https://doi.org/10.1126/science.1157996>.
16. A.A. Balandin, S. Ghosh, W. Bao, I. Calizo, D. Teweldebrhan, F. Miao and C.N. Lau, Superior Thermal Conductivity of Single-Layer Graphene, *Nano Lett.*, **8**, 902 (2008); <https://doi.org/10.1021/nl0731872>.
17. P. Manjunatha, Y.A. Nayaka, B.K. Chethana, C.C. Vidyasagar and R.O. Yathisha, Sensing And Bio-sensing Research Development of Multi-Walled Carbon Nanotubes Modified Pencil Graphite Electrode for the Electrochemical Investigation of Aceclofenac Present in Pharmaceutical and Biological Samples, *Sens. Bio-Sensing Res.*, **17**, 7 (2018); <https://doi.org/10.1016/j.sbsr.2017.12.001>.
18. K. Ojha, O. Anjaneyulu and A.K. Ganguli, Graphene-Based Hybrid Materials: Synthetic Approaches and Properties, *Curr. Sci.*, **107**, 397 (2014).
19. C.C. Vidyasagar, Y.A. Naik, T.G. Venkatesh and R. Viswanatha, Solid-State Synthesis and Effect of Temperature on Optical Properties of Cu-ZnO, Cu-CdO and CuO Nanoparticles, *Powder Technol.*, **214**, 337 (2011); <https://doi.org/10.1016/j.powtec.2011.08.025>.
20. H. Jiang, Chemical Preparation of Graphene-based Nanomaterials and their Applications in Chemical and Biological Sensors, *Small*, **7**, 2413 (2011); <https://doi.org/10.1002/smll.201002352>.
21. C.C. Vidyasagar, G. Hosamani and P. Kariyajjanavar, One-Pot Microwave Synthesis and Effect of Cu²⁺ Ions on Structural Properties of Cu-ZnO Nano Crystals, *Mater. Today Proc.*, **5**, 22171 (2018); <https://doi.org/10.1016/j.matpr.2018.06.582>.
22. S. Yang, X. Feng and K. Müllen, Sandwich-Like, Graphene-Based Titania Nanosheets with High Surface Area for Fast Lithium Storage, *Adv. Mater.*, **23**, 3575 (2011); <https://doi.org/10.1002/adma.201101599>.
23. Q. Xiang, J. Yu and M. Jaroniec, Synergetic Effect of MoS₂ and Graphene as Cocatalysts for Enhanced Photocatalytic H₂ Production Activity of TiO₂ Nanoparticles, *J. Am. Chem. Soc.*, **134**, 6575 (2012); <https://doi.org/10.1021/ja302846n>.
24. R. Saravanan, S. Karthikeyan, V.K. Gupta, G. Sekaran, V. Narayanan and A. Stephen, Enhanced Photocatalytic Activity of ZnO/CuO Nanocomposite for the Degradation of Textile Dye on Visible Light Illumination, *Mater. Sci. Eng. C*, **33**, 91 (2013); <https://doi.org/10.1016/j.msec.2012.08.011>.
25. B. Luo, S. Liu and L. Zhi, Chemical Approaches toward Graphene-Based Nanomaterials and their Applications in Energy-Related Areas, *Small*, **8**, 630 (2012); <https://doi.org/10.1002/smll.201101396>.
26. K.A. Mkhoyan, A.W. Contryman, J. Silcox, D.A. Stewart, G. Eda, C. Mattevi, S. Miller and M. Chhowalla, Atomic and Electronic Structure of Graphene-Oxide, *Nano Lett.*, **9**, 1058 (2009); <https://doi.org/10.1021/nl8034256>.
27. N. Özer and F. Tepehan, Optical and Electrochemical Characteristics of Sol Gel Deposited Iron Oxide Films, *Sol. Energy Mater. Sol. Cells*, **56**, 141 (1999); [https://doi.org/10.1016/S0927-0248\(98\)00152-4](https://doi.org/10.1016/S0927-0248(98)00152-4).
28. C.N.R. Rao, A.K. Sood, K.S. Subrahmanyam and A. Govindaraj, Graphene: The New Two-Dimensional Nanomaterial, *Angew. Chem. Int. Ed.*, **48**, 7752 (2009); <https://doi.org/10.1002/anie.200901678>.
29. M. Khan, A.H. Al-Marri, M. Khan, M.R. Shaik, N. Mohri, S.F. Adil, M. Kuniyil, H.Z. Alkhatlan, A. Al-Warthan, W. Tremel, M.N. Tahir and M.R.H. Siddiqui, Green Approach for the Effective Reduction of Graphene Oxide using *Salvadora persica* L. Root (Miswak) Extract, *Nanoscale Res. Lett.*, **10**, 1 (2015); <https://doi.org/10.1186/s11671-015-0987-z>.
30. J.S.Y. Chia, M.T.T. Tan, P.S. Khiew, J.K. Chin, H. Lee, D.C.S. Bien and C.W. Siong, A Novel One Step Synthesis of Graphene via Sonochemical-Assisted Solvent Exfoliation Approach for Electrochemical Sensing Application, *Chem. Eng. J.*, **249**, 270 (2014); <https://doi.org/10.1016/j.cej.2014.03.081>.
31. E. Murray, S. Sayyar, B.C. Thompson, R. Gorkin III, D.L. Officer and G.G. Wallace, A Bio-friendly, Green Route to Processable, Biocompatible Graphene/Polymer Composites, *RSC Adv.*, **5**, 45284 (2015); <https://doi.org/10.1039/C5RA07210G>.
32. C. Hu, T. Lu, F. Chen and R. Zhang, A Brief Review of Graphene-Metal Oxide Composites Synthesis and Applications in Photocatalysis, *J. Chinese Adv. Mater. Soc.*, **1**, 21 (2013); <https://doi.org/10.1080/22243682.2013.771917>.
33. C.C. Vidyasagar, Y.A. Naik, T.G. Venkatesha and P. Manjunatha, Sol-Gel Synthesis Using Glacial Acetic Acid and Optical Properties of Anatase Cu-TiO₂ Nanoparticles, *J. Nanoeng. Nanomanuf.*, **2**, 91 (2012); <https://doi.org/10.1166/jnan.2012.1058>.
34. N. Yusoff, N.M. Huang, M.R. Muhamad, S.V. Kumar, H.N. Lim and I. Harrison, Hydrothermal Synthesis of CuO/Functionalized Graphene Nanocomposites for Dye Degradation, *Mater. Lett.*, **93**, 393 (2013); <https://doi.org/10.1016/j.matlet.2012.10.015>.
35. B. Cao, S. Cao, P. Dong, J. Gao and J. Wang, High Antibacterial Activity of Ultrafine TiO₂/Graphene Sheets Nanocomposites under Visible Light Irradiation, *Mater. Lett.*, **93**, 349 (2013); <https://doi.org/10.1016/j.matlet.2012.11.136>.
36. J. Zhang, Z. Xiong and X.S. Zhao, Graphene-Metal-Oxide Composites for the Degradation of Dyes Under Visible Light Irradiation, *J. Mater. Chem.*, **21**, 3634 (2011); <https://doi.org/10.1039/c0jm03827j>.
37. A. Chidembo, S.H. Aboutaleb, K. Konstantinov, M. Salari, B. Winton, S.A. Yamini, I.P. Nevirkovets and H.K. Liu, Globular Reduced Graphene Oxide-Metal Oxide Structures for Energy Storage Applications, *Energy Environ. Sci.*, **5**, 5236 (2012); <https://doi.org/10.1039/C1EE02784K>.

38. L. Richtera, D. Chudobova, M. Kremplova, V. Milosavljevic, P. Kopel, K. Cihalova, I. Blazkova, D. Hynek, V. Adam and R. Kizek, The Composites of Graphene Oxide with Metal or Semimetal Nanoparticles and their Effect on Pathogenic Microorganism, *Materials*, **8**, 2994 (2015); <https://doi.org/10.3390/ma8062994>.
39. S. Botta, J. Navio, M. Hidalgo, G.M. Restrepo and M.I. Litter, Photocatalytic properties of ZrO₂ and Fe/ZrO₂ semiconductors Prepared by a Sol-Gel Technique, *J. Photochem. Photobiol. A Chem.*, **129**, 89 (1999); [https://doi.org/10.1016/S1010-6030\(99\)00150-1](https://doi.org/10.1016/S1010-6030(99)00150-1).
40. Y. Hu, J. Jin, P. Wu, H. Zhang and C. Cai, Graphene-Gold Nanostructure Composites Fabricated by Electrodeposition and their Electrocatalytic Activity toward the Oxygen Reduction and Glucose Oxidation, *Electrochim. Acta*, **56**, 491 (2010); <https://doi.org/10.1016/j.electacta.2010.09.021>.
41. R. Liu, S. Li, X. Yu, G. Zhang, S. Zhang, J. Yao, B. Keita, L. Nadjjo and L. Zhi, Facile Synthesis of Au-nanoparticle/Polyoxometalate/Graphene Tricomponent Nanohybrids: An Enzyme-Free Electrochemical Biosensor for Hydrogen Peroxide, *Small*, **8**, 1398 (2012); <https://doi.org/10.1002/smll.201102298>.
42. C. Zhu, J. Zhai, D. Wen and S. Dong, Graphene Oxide/Polypyrrole Nanocomposites: One-step Electrochemical Doping, Coating and Synergistic Effect for Energy Storage, *J. Mater. Chem.*, **22**, 6300 (2012); <https://doi.org/10.1039/c2jm16699b>.
43. S. Rout, M.S.c Thesis, Synthesis and Characterization of CuO/Graphene Oxide Composite, National Institute of Technology, Rourkela, India (2013).
44. P. Benjwal, M. Kumar, P. Chamoli and K.K. Kar, Enhanced Photocatalytic Degradation of Methylene Blue and Adsorption of Arsenic(III) by Reduced Graphene Oxide (rGO)-Metal Oxide (TiO₂/Fe₃O₄) based nanocomposites, *RSC Adv.*, **5**, 73249 (2015); <https://doi.org/10.1039/c5ra13689j>.
45. Y. Ma and J.-N. Yao, Photodegradation of Rhodamine B Catalyzed by TiO₂ Thin Films, *J. Photochem. Photobiol. A Chem.*, **116**, 167 (1998); [https://doi.org/10.1016/S1010-6030\(98\)00295-0](https://doi.org/10.1016/S1010-6030(98)00295-0).